 doi:10.20944/preprints202206.0348.v1

Article

Molecular Basis of Inhibitory Mechanism of Naltrexone and Its Metabolites through Structural and Energetic Analyses

Martiniano Bello

Laboratorio de Diseño y Desarrollo de Nuevos Fármacos e Innovación Biotecnológica, Escuela Superior de Medicina, Instituto Politécnico Nacional, Plan de San Luis y Diaz Mirón, s/n, Col. Casco de Santo Tomas, Ciudad de México 11340, México.
Correspondence: mbellor@ipn.mx

Abstract:

Naltrexone (NTX) is a potent opioid antagonist with good blood-brain barrier permeability, targeting different endogenous opioid receptors, particularly the mu-opioid receptor (MOR). Therefore, it represents a promising candidate for drug development against drug addiction. However, the details of the molecular interactions of NTX and its derivatives with MOR are not fully understood, hindering ligand-based drug discovery. In the present study, taking advantage of the high-resolution X-ray crystal structure of the murine MOR (mMOR), we constructed a homology model of the human MOR (hMOR). A solvated phospholipid bilayer was built around the hMOR and submitted to microsecond (μs) molecular dynamics (MD) simulations to obtain an optimized hMOR model. NTX and its derivatives were docked into the optimized hMOR model and submitted to μs MD simulations in an aqueous membrane system. The MD simulation results were submitted to Molecular Mechanics Generalized-Born surface area (MMGBSA) binding free energy calculations and principal component analysis. Our results revealed that NTX and its derivatives showed differences in protein-ligand interactions; however, they shared contact with residues at TM2, TM3, H6, and TM7. The binding free energy and principal component analysis revealed the structural and energetic effects responsible for the higher potency of NTX compared to its derivatives.

Keywords: Naltrexone; mu-opioid receptor; MD simulations; MMGBSA; binding free energy

1. Introduction

Naltrexone (NTX) has been employed for decades as a therapy for alcoholism [1-4] and opiate dependency [5-7], with well-controlled clinical studies establishing it as an efficacious medication for the treatment of alcoholism [2,8-9]. A major disappointment of its employment has been that it is known to undergo a fast and extensive hepatic metabolism after administration. NTX is a potent opioid antagonist, targeting endogenous opioid receptors (mu, delta, and kappa receptors), but particularly the mu-opioid receptors (MOR) [10-11]. MOR belongs to the rhodopsin family of G-protein coupled receptors (GPCRs), and it has been confirmed that the rhodopsin structure has a heptahelical domain on both sides of the plasma membrane [12-15].

 doi:10.20944/preprints202206.0348.v1

Therefore, due to the lack of X-ray crystallography data for human MOR (hMOR), the seven transmembrane (TM) motifs of rhodopsin has been considered an appropriate model for other GPCRs [16-17]. However, the low sequence identity between opioid receptors and rhodopsin (30%) could be inconvenient for the construction of opioid receptor models based on the rhodopsin X-ray crystal structure through homology modeling.

Crystallographic studies have provided structural data on inactive, active, and fully active structures of murine MOR (mMOR) conformation. The crystal structure of inactive mMOR was co-crystallized with the morphine-like antagonist β-FNA [18]. This structure enabled the development of different theoretical studies to explore rational drug design [19-20] and structural changes associated with MOR activation [21-22]. More recently, a high-resolution crystal structure of the mMOR bound to the morphine-like agonist BU72 [23] and one stabilizing G protein mimetic camelid antibody fragment (Nb39) [24-26] was crystallized, providing more structural evidence about the activation of MOR that is linked with its therapeutic function. This high-resolution mMOR structure and the high sequence identity (97%) with hMOR provide a unique chance to construct hMOR homology models for the evaluation of its binding between NTX and its derivatives.

Molecular dynamics (MD) simulation studies have provided relevant information about the MOR activation mechanism, taking the active or inactive MOR state as the initial conformer [23, 27-31]. Based on these studies, we know that the active form of mMOR shows the following features compared with the inactive state: 1) a sizeable outward motion of TM6 relative to TM3; 2) minor inner motion of TM5 and TM7; 3) breakage of the hydrogen bond between Arg165 and Thr279 (equivalent to the $Arg^{3.50}$–$Asp/Glu^{6.30}$ GPCR ionic lock); and 4) formation of one hydrogen bond between Arg165 and Tyr252.

The major metabolite of NTX in humans and other animal species is 6-β-naltrexol (NTXOL), and 2-hydroxy-3-O-methylnaltrexol (HMNTXOL) is another minor metabolite. NTXOL is also an opioid receptor agonist but is hundreds of times less potent than NTX at the mu-receptor [32]. Molecular modeling analysis based on molecular mechanics and semi-empirical calculations has shown that NTXOL and NTX share a comparable surface area and volume, indicating that both substrates may have a similar affinity for the same binding site in opioid receptors [33].

In this study, we explore the structural and energetic basis of the mMOR in complex with NTX and its derivatives. First, hMOR was constructed through homology modeling methods employing the high-resolution mMOR structure. The hMOR was anchored in a solvated phospholipid bilayer and submitted to one microsecond (μs) MD simulation to obtain an optimized hMOR model. Clustering analysis allowed the most populated hMOR conformer to be obtained, which was then used to perform docking studies and obtain hMOR-ligand complexes with NTX and its derivatives. The hMOR-ligand complexes were also built in an aqueous membrane system and submitted to μs MD simulations. These were followed by analyses relating to

 doi:10.20944/preprints202206.0348.v1

the binding free energies with the molecular mechanics Generalized-Born surface area (MMGBSA) approach and principal component (PC) analysis.

2. Results

2.1 Docking results

The docking studies showed the lowest binding free energy for the hMOR-NTX, hMOR-NTXOL, and hMOR-HMNTXOL complexes (Fig. 1). For the hMOR-NTX complex, the ligand formed contacts with transmembrane helixes TM3, TM5, TM6, and TM7 through seven hydrophobic interactions (W135, I146, M153, V238, W295, I298, and V302), one charge residue (D149), and three polar residues (Y150, H299, and Y328). D149 in TM3 (equivalent to D147 in mMOR) also established two hydrogen bonds and one salt bridge with the protonated nitrogen atom of NTX (Fig. 1A).

In the hMOR-NTXOL complex, NTXOL was coupled by six hydrophobic contacts: L58, L221, I298, V302, W320, and I324. Polar interactions were mediated by one charged and five polar residues: D149, T122, Q126, Y150, T220, and Y328 (Fig. 1B). These interactions correspond to the extracellular region (ER) (L58), TM2 (T122 and Q126), TM3 (D149 and Y150), TM6 (I298 and V302), and TM7 (W320, I324, and Y328).

Preprints (www.preprints.org) | NOT PEER-REVIEWED | Posted: 27 June 2022 doi:10.20944/preprints202206.0348.v1

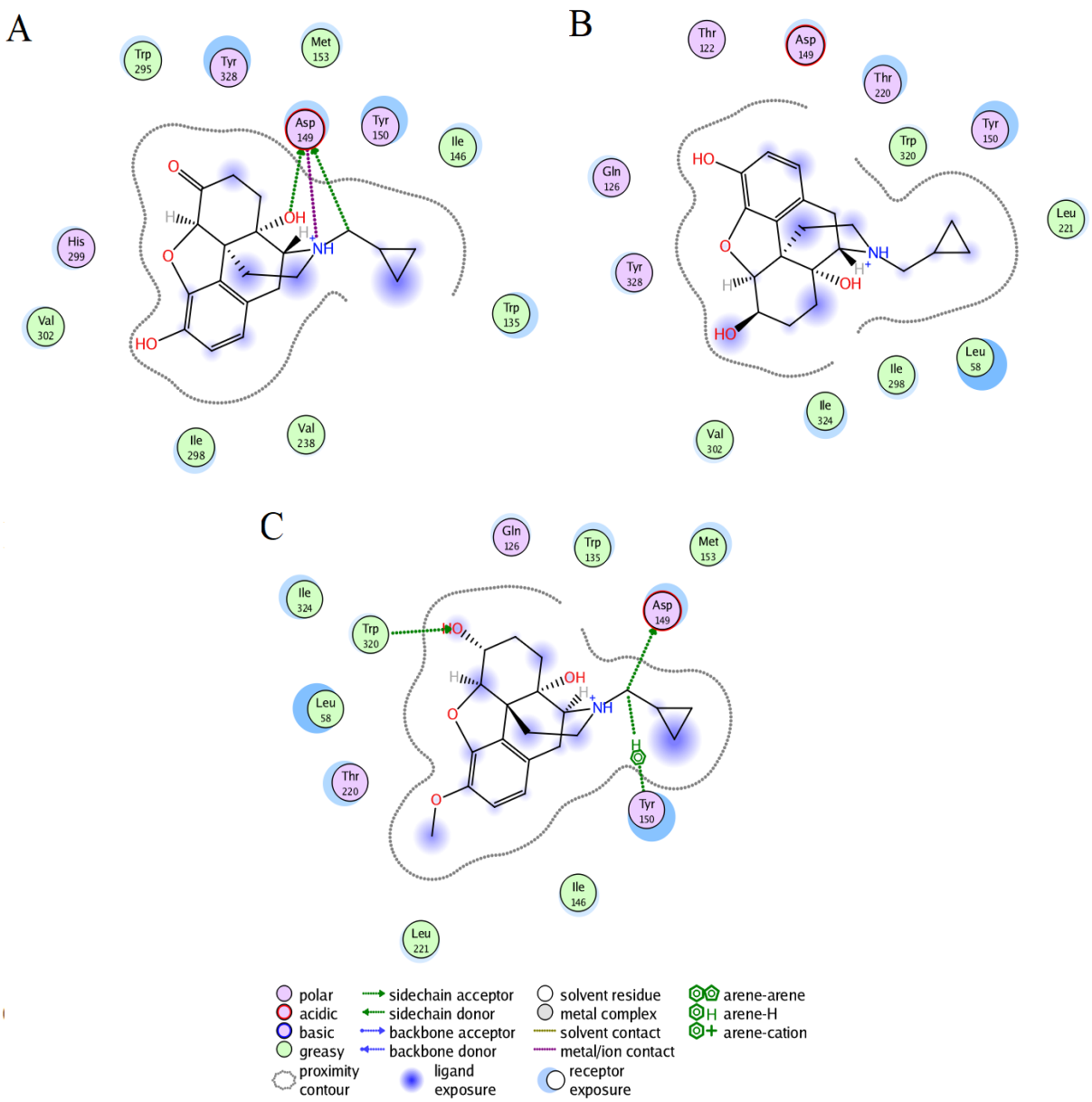

Fig. 1. Docking interactions of NTX, NTXOL, or HMNTXOL with hMOR. Interactions of NTX (A), NTXOL (B), or HMNTXOL (C) with hMOR.

The hMOR-HMNTXOL complex is stabilized by seven hydrophobic residues: L58, W135, M153, T220, L221, W320, and I324. The polar contacts were formed by Q126, D149, Y150, and T220 (Fig. 1C). These residues are placed along the ER (L58), TM2 (Q126), TM3 (D149, Y150, and M153), and TM7 (W320 and I324). From these polar residues, D149 and W320 formed hydrogen bonds with the ligand, whereas Y150 formed arene-H interactions. The hMOR-NTX, hMOR-NTXOL, and hMOR-HMNTXOL complexes were built in an aqueous membrane system and submitted to μs MD simulations to explore the molecular recognition under a dynamic and solvated environment.

 doi:10.20944/preprints202206.0348.v1

2.2 Stability of the systems

Before analyzing the results, we evaluated different geometrical parameters (the area per lipid headgroup, RMSD, and Rg) to observe whether the system was appropriately equilibrated. The area per lipid analysis allowed us to evaluate the bilayer thickness. Fig. 2SA shows the time evolution of the area per lipid for the free and bound systems. This figure indicates that the systems exhibit higher area per lipid values at the beginning of the simulations, dropping off to a converged value within 0.15 µs, with average area per lipid values of 68.56, 69.56, 69.73, and 70.27 $Å^2$ for the free hMOR, hMOR-NTX, hMOR-NTXOL, and hMOR-HMNTXOL systems, respectively, which are in line with the values reported for other protein-POPC-membrane systems [34]. Fig. 1SB shows that free hMOR reached equilibrium between 0.3 and 0.4 µs, with average RMSD values of 10.0 Å. The hMOR-ligand systems reached equilibrium between 0.1 and 0.2 µs, with RMSD values of 2.9, 4.0, and 4.1 Å for the hMOR-NTX, hMOR-NTXOL, and hMOR-HMNTXOL systems, respectively (Fig. S1B). The significant difference in RMSD values between the free and bound hMOR systems is due to the hMOR-ligand systems were started from a pre-equilibrated hMOR conformer obtained over the equilibrated simulation of free hMOR system. Fig. 1SC shows that the free and bound hMOR systems reached constant Rg values between 0.1 and 0.4 µs, with average values of about 25.5 Å. Based on these results, the first 0.4 µs were discarded from further analysis.

2.3 Ligand interactions on the hMOR-ligand complex through MD simulations

The most populated conformers through clustering analysis showed representative interactions of the three complexes. NTX at the hMOR binding was bound by six hydrophobic residues at TM2 (A119), a loop connecting TM2-TM3 (W135), TM3 (M153), TM6 (W295 and I298), and TM7 (I324). The polar interactions were established by nine residues at TM2 (D116 and Q126), TM3 (D149 and N152), TM6 (H299), and TM7 (G327, Y328, N330, and S331). From these residues, D149 also formed one hydrogen bond and a salt bridge with the amine protonated atom of NTX (Fig. 2A).

Preprints (www.preprints.org) | NOT PEER-REVIEWED | Posted: 27 June 2022 doi:10.20944/preprints202206.0348.v1

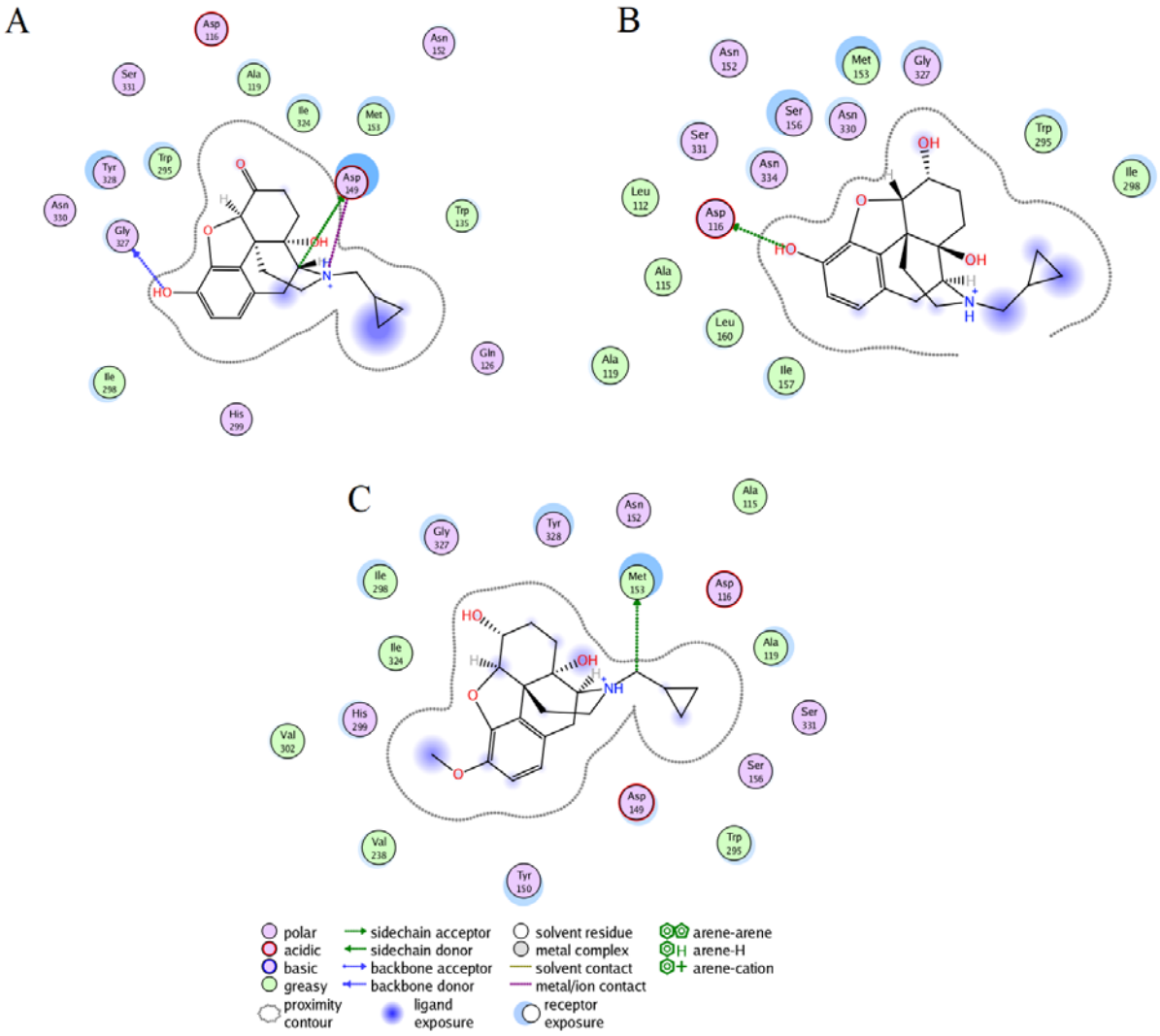

Fig. 2. Protein-ligand interactions of NTX, NTXOL, or HMNTXOL with hMOR. Interactions of NTX (A), NTXOL (B), or HMNTXOL (C) with hMOR present in the most populated conformations through MD simulations.

The hMOR-NTXOL complex was coupled by eight hydrophobic residues at TM2 (L112, A115, and A119), TM3 (M153, I157, and L160), and TM6 (W295 and I298). It was also stabilized by seven polar interactions at TM2 (D116), TM3 (N152 and S156), and TM7 (G327, N330, S331, and N334). Of these, D116 forms a salt bridge with NTXOL (Fig. 2B).

The hMOR-HMNTXOL complex is coordinated by eight hydrophobic residues at TM2 (A115 and A119), TM3 (M153), TM5 (V238), TM6 (W295, I298, and V302), and TM7 (I324). M153 also forms one hydrogen bond with NTX. The polar contacts were formed by residues at TM2 (D116), TM3 (D149, Y150, N152, and S156), TM6 (H299), and TM7 (G327, Y328, and S331) (Fig. 2C). Comparative analysis of the most populated hMOR-NTX, hMOR-NTXOL, and hMOR-HMNTXOL complexes during MD simulations showed that the three complexes shared contact with nine residues: H2 (D116 and A119), H3 (N152, M153, and S156), H6

Preprints (www.preprints.org) | NOT PEER-REVIEWED | Posted: 27 June 2022 doi:10.20944/preprints202206.0348.v1

(W295 and I298), and H7 (G327 and S331). Comparison with docking results shows a higher number of residues in common among the three simulated complexes (Fig. 1 and Fig. 2).

2.4 Binding free energy calculations

Binding free energy (ΔG_{mmgbsa}) values were determined using the MMGBSA approach and were energetically favorable for the three hMOR-ligand complexes (Table 1). Table 1 also shows that the interaction energy (ΔE_{MM}) was energetically more favorable for NTX than for NTXOL and HMNTXOL. The solvation free energy ($\Delta G_{solv\text{-}GBSA}$) contributed unfavorably to the ΔG_{mmgbsa} for the three complexes. The $\Delta G_{solv\text{-}GBSA}$ values suggest that NTX exhibits a higher desolvation cost than NTXOL and HMNTXOL, which contributes to the decrease in its ΔG_{mmgbsa} value. The ΔG_{mmgbsa} values were thermodynamically more favorable for NTX than for NTXOL and HMNTXOL, explaining the higher affinity of NTX.

Table 1. Binding free energy components for protein-ligand interactions of hMOR-NTX, hMOR-NTXOL, and hMOR-HMNTXOL systems calculated using the MMGBSA approach (values in kcal/mol).

Systems	ΔE_{MM}	$\Delta G_{solv\text{-}GBSA}$	ΔG_{MMGBSA}
hMOR-NTX	-71.36 ± 7.12	37.97 ± 6.11	-33.39 ± 2.68
hMOR-NTXOL	-39.43 ±11.8	8.76 ± 1.0	-30.67 ± 2.95
hMOR-HMNTXOL	-49.99 ± 8.5	20.36 ± 8.7	29.63 ± 2.62

2.5 Per-residue free energy decomposition for the mu-receptor-NTX complex

Table 1S, supplementary material displays the energies for each residue involved in the protein-ligand interactions of the hMOR-ligand systems. In the hMOR-NTX system, the major source of the binding free energy (ΔG_{mmgbsa} ≥1.0 Kcal) were M153, W295, I298, I324, G327, and Y328 (Table 2). Of these residues, G327 participates in forming hydrogen bonds through its polar backbone atoms (Fig. 2A), M153, W295, I298, and I324 stabilize through hydrophobic interactions, and Y328 stabilizes by polar interactions. In the hMOR-NTXOL system, A115, A119, M153, I157, W295, N330, and N334 were the major contributors to ΔG_{mmgbsa}. A115, A119, M153, I157, and W295 participate by forming hydrophobic contacts, and N330 and N334 by polar contacts (Fig. 2B). For the hMOR-HMNTX system, M153, I298, I324, and Y328 mostly contributed to the binding affinity, of which M153 formed hydrophobic and one hydrogen bond with HMNTXOL, I298 and I324 formed hydrophobic contacts, and Y328 formed polar interactions (Fig. 2C). A comparison of the ligand stabilization on the three systems indicates that NTX and NTXOL are better stabilized at the mu-receptor binding site than HMNTXOL, in line with the ΔG_{mmgbsa} values (Table 1). In the hMOR-NTX and hMOR-NTXOL systems, there were a similar number of residues contributing most to the affinity, but the residues were different; only M153 and W295 were shared in both complexes. In fact, the hMOR-NTX and hMOR-HMNTXOL systems shared contacts through a higher number of common residues (M153, I298, I324, and Y328) than the hMOR-NTXOL.

Table 2. Per-residue free energy for hMOR-ligand interaction complexes (values in kcal/mol).

Residue	hMOR-NTX	hMOR-NTXOL	hMOR-HMNTXOL
A115		-1.173	

Preprints (www.preprints.org) | NOT PEER-REVIEWED | Posted: 27 June 2022 doi:10.20944/preprints202206.0348.v1

A119		-1.128	
M153	-1.780	-1.551	-3.050
I157		-1.016	
W295	-1.572	-1.176	
I298	-1.184		-1.725
I324	-1.216		-1.382
G327	-1.547		
Y328	-2.774		-1.522
N330		-1.566	
N334		-1.942	

2.6 Principal component (PC) analysis

PC analysis identified the most important eigenvectors. For free and bound hMOR systems, the first two eigenvectors (PC1 and PC2) comprise the largest eigenvalues, containing 44.0, 69.0, 31.0, and 48.8% of the total mobility of free hMOR, hMOR-NTX, hMOR-NTXOL, and hMOR-HMNTXOL, respectively. Therefore, these eigenvectors have the main conformational states sampled during the simulations for the four systems (Fig. 3). Projection onto the phase space of PC2 vs. PC1 shows that free hMOR (Fig. 3A) covers a bigger region in the essential subspace than hMOR-NTX (Fig. 3B), indicating that the latter has a lower conformational entropy compared to free hMOR. Fig. 3C indicates that hMOR-NTXOL covers a significantly larger region in the essential subspace than free hMOR, suggesting a larger conformational entropy for hMOR-NTXOL. Fig. 3D highlights that hMOR-HMNTXOL exhibits a similar distribution in the essential subspace than free hMOR, indicative of similar conformational behavior for these two systems. The diagonalized covariance matrix of backbone heavy atoms demonstrated the following values: hMOR (29.2 nm^2), hMOR-NTX (18.6 nm^2), hMOR-NTXOL (41.5 nm^2), and hMOR-HMNTXOL (26.2 nm^2). These values indicate that the binding of NTX to hMOR contributes to decreasing the number of conformational states. In contrast, the binding of NTXOL increases the number of conformational states present in solution, whereas the binding of HMNTXOL to the hMOR binding site does not significantly impact the number of conformational states with respect to the free state.

Graphical representation of the total fluctuation along PC1 shows that the free and bound hMOR systems exhibit the highest collective motions along the extracellular domain, cytoplasmic domain, and the loop between TM5 and TM6 (Loop TM5-TM6) for the free hMOR (Fig. 4A), hMOR-NTX (Fig. 4B), and hMOR-NTXOL (Fig. 4C) systems, but only along the extracellular and cytoplasmic domains for hMOR-HMNTXOL (Fig. 4D). hMOR-NTXOL exhibits the highest collective motions along the three abovementioned regions compared to free hMOR, hMOR-NTX, and hMOR-NTXOL (Fig. 4C), systems, supporting the high heterogeneity observed through visualization onto the essential space (Fig. 3C). It is also appreciated that the reduction in conformational mobility of free hMOR-NTX compared to free hMOR took place along the

Preprints (www.preprints.org) | NOT PEER-REVIEWED | Posted: 27 June 2022 doi:10.20944/preprints202206.0348.v1

extracellular domain, whereas similar mobility along the extracellular domain is observed for free hMOR and hMOR-HMNTXOL, but in the opposite direction.

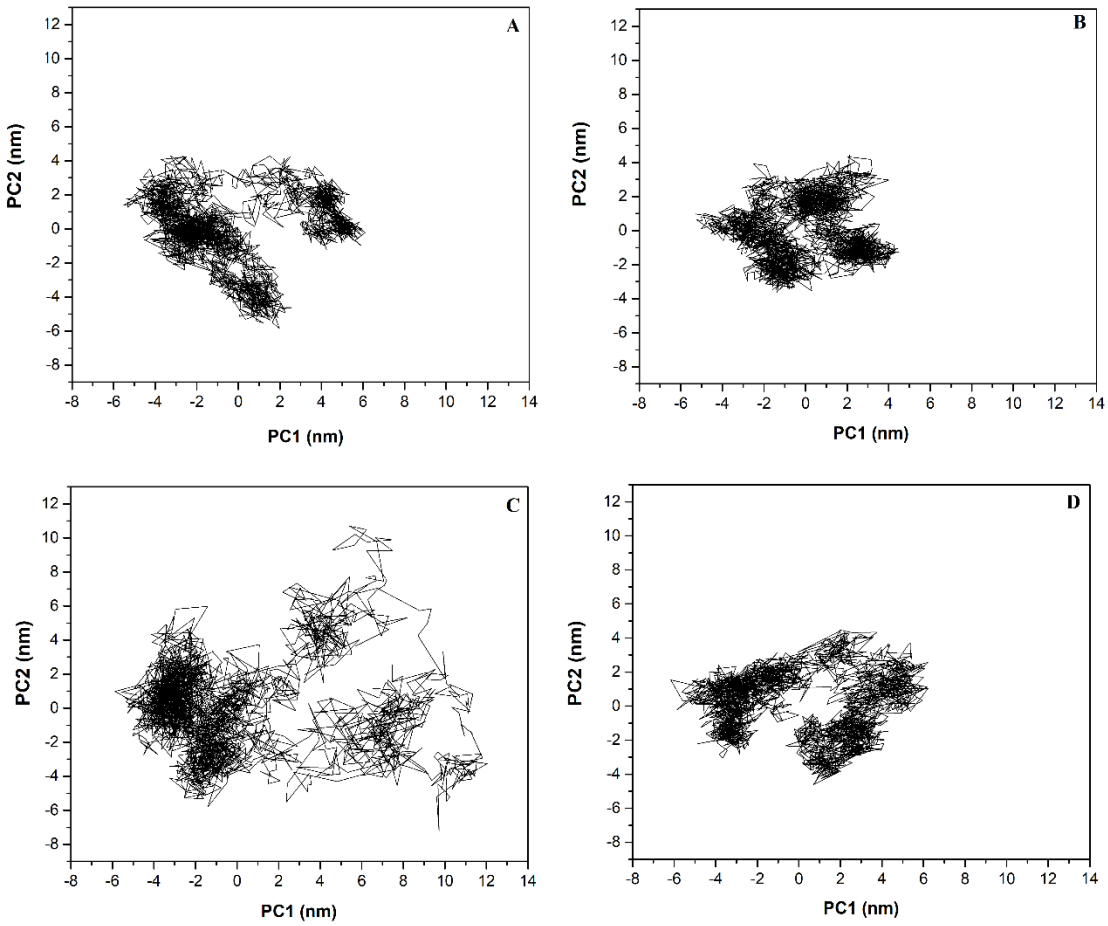

Fig. 3. Projection of the free and bound hMOR systems in phase space. Projection of the motion in the phase space along PC2 vs. PC1 for free hMOR (A), hMOR-NTX (B), hMOR-NTXOL (C), and hMOR-HMNTXOL (D).

Preprints (www.preprints.org) | NOT PEER-REVIEWED | Posted: 27 June 2022 doi:10.20944/preprints202206.0348.v1

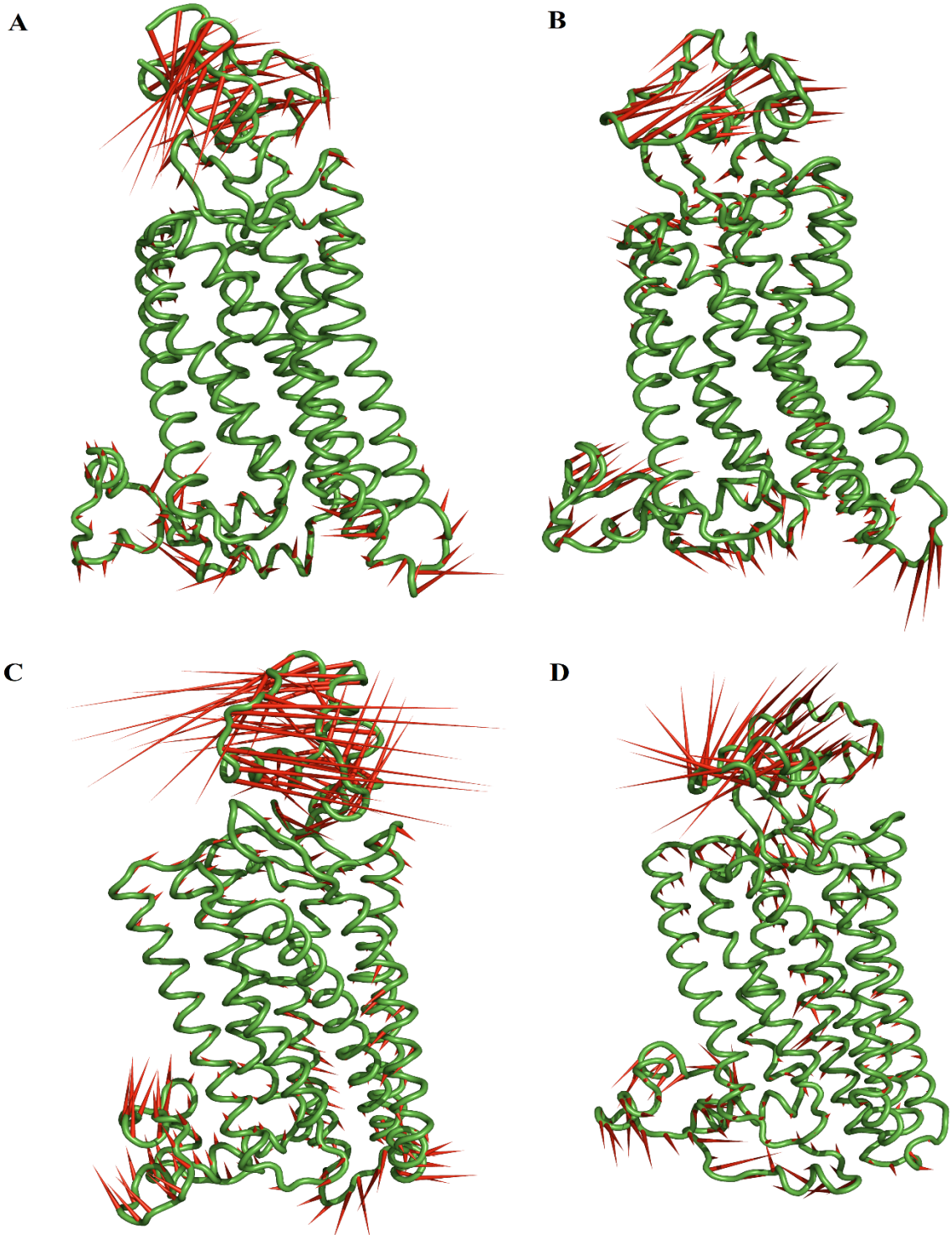

Fig. 4. Graphic representation of the two extreme projections of the free and bound hMOR systems. Graphical depiction of the two extreme projections along PC1 vs PC2 for the free hMOR (A), hMOR-NTX (B), hMOR-NTXOL (C), and hMOR-HMNTXOL (D) systems. The direction and magnitude of motions are depicted as porcupine depictions.

3. Discussion

Experimental studies by X-ray crystallography have shed insight into the active and inactive state of mMOR [18,23]. This structural data enabled the development of different theoretical studies, such as rational drug design, and exploration of the conformational changes associated with MOR activation [19,20-22,27-31].

 doi:10.20944/preprints202206.0348.v1

However, there is currently no crystallographic information for hMOR. Homology modeling studies have therefore been implemented to obtain hMOR, and these have been employed to explore structural changes present between the agonist or antagonist and hMOR [35-37]. In this study, we employed the high-resolution mMOR structure that has a high sequence identity (97%) with hMOR, along with its active state, to construct our hMOR homology model. Since hMOR is a membrane receptor, a complete membrane-aqueous system containing the modeled hMOR was built to optimize the receptor structure through 1 μs MD simulation. Based on cluster analysis over the equilibrated simulation time, the most populated hMOR conformer was selected to perform docking studies with NTX, NTXOL, or HMNTXOL. These hMOR-ligand complexes were also simulated in a membrane-aqueous environment through one μs MD simulations to relax and optimize binding interactions between the ligand and the amino acid residues in the hMOR binding cavity.

Docking studies showed that only four contacts were shared among the hMOR-NTX, hMOR-NTXOL, and hMOR-HMNTXOL complexes: I298, V302, D149, and Y150. Protein-ligand interactions involving D149 and Y150 have also been observed for complexes between hMOR in inactive, active, and full-active states with morphine, fentanyl, or NTX [35]. In fact, hMOR-NTXOL and hMOR-HMNTXOL shared a higher number of contacts (L58, Q126, Y150, D149, I298, V302, W320, and I324) than hMOR-NTX. This agrees with previous molecular mechanics and semi-empirical calculations that suggested a similar affinity between NTX or NTXOL with hMOR, based on the comparable surface area and volume [33].

We also observed differences in the type of residues stabilizing the three complexes after MD simulations; however, several residues present in the docking calculations were still present during MD simulations: residues at loop TM2-TM3 (W135), TM3 (D149, Y150, and M153), TM5 (V238), TM6 (W295, I298, H299, and V302), and TM7 (I324 and Y328). The salt bridge formed between D149 (D147 in mMOR) and the protonated nitrogen atom of ligand (Fig. 1A), which was only observed for the hMOR-NTX complex, is an interaction previously inferred from experimental studies [38]. This interaction also favors interactions between TM3 and TM7 through one hydrogen bond between D149 and Y326 and MOR activation [38-41]. Interactions involving TM3 (M153), TM5 (V238), TM6 (H299 and V302), and TM7 (Y328) have also been reported for the hMOR-NTX complex through theoretical studies combining docking and MD simulations [35]. On the other hand, interactions with Y328 have been observed in MOR-agonist/antagonist complexes, and it has therefore been suggested that interactions with this residue could be associated with affinity rather than with efficacy [35]. Interactions with Y328 (Y326 in mMOR) may also be critical for the molecular recognition of NTX by hMOR, since residue mutation to phenylalanine decreases the affinity of NTX to mMOR [42].

ΔG_{mmgbsa} values determined using the MMGBSA method showed that the binding affinity was energetically more favorable for NTX than for its derivatives, explaining the higher potency of NTX compared with

 doi:10.20944/preprints202206.0348.v1

NTXOL, which is also a MOR antagonist but a hundred times less potent than NTX [32]. However, despite NTXOL showing a lower affinity, many other factors contribute to its lower potency, such as entropic effects, which we didn't explore with the MMGBSA approach.

Per-residue decomposition analysis indicated that NTX and NTXOL are better stabilized at the MOR binding site than HMNTXOL, in line with the ΔG_{mmgbsa} values (Table 1). In the MOR-NTX and MOR-NTXOL systems, the quantity of residues that mainly contribute to the affinity were similar, but they were of a different type; only M153 and W295 were shared in both complexes. In fact, the MOR-NTX and MOR-HMNTXOL systems shared more common contacts (M153, I298, I324, and Y328) than they shared with NTXOL.

PC analysis suggests that the favorable entropy contribution observed for the MOR-NTXOL complex could contribute to further decreasing the affinity predicted through the binding free energies reported in Table 1. In contrast, the unfavorable entropy observed for the MOR-NTX complex may impact favorably on the reported binding affinity. Meanwhile, no important changes should be expected for the hMOR-HMNTXOL complex, since there are no important conformational changes with respect to free hMOR.

4. Material and methods

4.1 Structural modeling

The hMOR structure was constructed using homology modeling procedures. Modeler 9.17 [43] was used to build the hMOR model, using the high-resolution crystal structures of mMOR (PDB entry 5C1M_chainA) in the active state as a template, whose sequence (Uniprot, P42866) is 97.0% identical to human MOR (Uniprot, P35372). The best hMOR model was selected from this analysis based on the DOPE score of MODELLER Version 9.14. The model was subjected to MolProbity analysis [44], reporting residues in favored regions of the Ramachandran plot. This structure was built in an aqueous membrane system and submitted to 1 μs MD simulations to optimize the internal interactions.

4.2 Docking studies

The structures of NTX, NTXOL, and HMNTXOL were taken from ChemSpider (http://www.chemspider.com/) and optimized at the AM1 level with Gaussian 09W software [45]. The hMOR used to perform the docking calculations was obtained over the equilibrated simulation time (last 0.6 μs) through a clustering analysis of 1 μs MD simulations (Fig. 1S). Docking studies were carried out using AutoDock Tools 1.5.6 and AutoDock 4.2 programs [46]. Hydrogen bonds and Gasteiger partial charges were assigned to ligands, and Kollman partial charges were placed on protein atoms. The Lamarckian-genetic

 doi:10.20944/preprints202206.0348.v1

algorithm with an initial randomized population of 100 individuals and a maximum number of energy evaluations of 1 x 10^7 was employed to generate binding poses. A grid box with a spacing of 0.375 and a size of 70 x 70 x 70 Å was constructed around the binding site to establish the ligand search location. The most populated cluster for the hMOR-ligand conformer, together with the lowest energy binding pose, was selected as the starting conformation for MD simulations. The docking protocol was validated by docking the co-crystallized ligand in mMOR (PDB entry 5C1M_chainA) in the most populated hMOR conformer obtained through MD simulations (section 2.1). The root means squared deviation (RMSD) of the docked pose with the lowest free energy was about 2.0 Å (Fig. 1S), indicating that the model remains near the initial conformation throughout MD simulation, supporting its use of reliable starting points to evaluate the ligand-binding impact.

4.3 Anchoring of the receptor-ligand complex onto the membrane

Orientation of the receptor-ligand complex with respect to the membrane was carried out using the OPM (Orientations of Proteins in Membranes) server [47]. A rectangular pre-equilibrated POPC (1-palmitoyl-2-oleoyl-sn-glycero-3-phosphocholine) membrane of dimensions 106.9 x 107.2 x 134.0 Å (xyz) was generated for each system using the membrane-builder tool of CHARM [48-49]. The replacement method was used to place the receptor-ligand complex into the POPC membrane, which was comprised of 290 POPC phospholipids. The protein-receptor-membrane system was solvated with 31068 TIP3 water molecules and neutralized with 0.15 M NaCl using the ion placing method.

4.4 MD simulations

The protein-receptor-membrane systems were submitted to MD simulations using the Amber 16 package [50]. Ligand parameters were obtained using the Generalized Amber Force Field (GAFF), considering the AM1-BCC method and GAFF to assign atomic charges. Topologies for the systems were constructed with a Leap module using ff14SB [51], Lipid14 [52], and GAFF [53]. The systems were energy minimized with position restraints on the protein-receptor-membrane atoms, allowing relaxation of the solvent. Systems were gradually heated from 0-310 K for one nanosecond (ns) under the NVT ensemble, with the restraint of the heavy atoms of the protein-receptor-membrane system. The system was equilibrated for one ns under the NPT ensemble at 310 K and 1 bar pressure with the restrained heavy atoms, followed by five ns with the entirely unrestricted system. Triplicate MD simulations were run for one µs for each system under periodic boundary conditions (PBCs) using an NPT ensemble at 310 K and 1 bar pressure. Long-range electrostatic interactions were treated with the particle mesh Ewald [54], considering a 10 Å cutoff for van der Waals interactions. The SHAKE algorithm [55] was used to restrict bond lengths at the equilibrium. Pressure was maintained using a semi-

 doi:10.20944/preprints202206.0348.v1

isotropic constant surface tension to preserve the area per lipid. The temperature was maintained using Langevin dynamics.

4.5 MD trajectory analysis

The area per lipid headgroup, the time dependent Cα RMSD, radius of gyration (Rg) and clustering analysis were estimated using AmberTools16. The equilibrated part of each simulation was concatenated into a single joined trajectory and employed to evaluate the PC analysis, clustering analysis, and binding free energy analysis. Figures were created using PyMOL [56].

4.6 Binding free energy

The binding free energies of the receptor-ligand interactions were calculated using the MMGBSA method [57]. The binding free energy was estimated over the equilibrated simulation time, saving 4000 receptor-ligand conformations. The solvation free energy was determined using implicit solvent models [58] and ionic strength of 0.15 M. The ΔG_{bind} values using the MMGBSA approach were estimated as reported elsewhere [59].

5. Conclusions

High resolution crystallographic structure data, homology modeling, docking, and MD simulations analyses were used to explore the thermodynamics and dynamic analysis of the molecular recognition of NTX and its derivatives with MOR. Clustering analysis showed that NTX and its derivatives were stabilized by residues at loop TM2-TM3, TM3, TM5, TM6, and TM7. However, the characteristic salt bridge between D149 at TM3 and the protonated nitrogen atom of NTX, which favors interactions between TM3 and TM7 and subsequent MOR activation, was only present for the hMOR-NTX complex. Thermodynamic and clustering analysis showed that NTX and its derivatives were bound at the hydrophobic cavity of MOR, with the binding free energy order of NTX ≥ NTXOL ≥ HMNTXOL, which correlates with the higher potency of NTX compared with NTXOL. Although structural analysis demonstrated that NTX and its derivatives shared contacts with a group of similar residues, per-residue decomposition analysis indicated that a major source of the affinity came from different residues for the hMOR-NTX and hMOR-HMNTX complexes. Finally, PC analysis revealed that the unfavorable entropy contribution observed for the hMOR-NTX complex may contribute to improving the binding affinity of NTX for hMOR, contrasting with the hMOR-NTXOL or hMOR-HMNTXOL complexes, where favorable or no conformational changes were observed in the molecular recognition for hMOR-NTXOL or hMOR-HMNTXOL, respectively.

Declarations

Funding: The work was supported by grants from CONACYT (A1-S-21278) and SIP/IPN (20220315).

Conflicts of interest/Competing interests: The author declares they have no conflict of interest in terms of the content of this manuscript.

Availability of data and material: The datasets supporting the conclusions of this research are contained within the paper and its additional files.
Code availability: Not applicable.
Authors' contributions: Not applicable.

References

1. Litten RZ, Allen JP. Advances in development of medications for alcoholism treatment. Psychopharmacology (Berl). 1998 Sep;139(1-2):20-33.
2. Volpicelli JR, Alterman AI, Hayashida M, O'Brien CP: Naltrexone in the treatment of alcohol dependence. Arch Gen Psychiatry 1992, 49:876–879.
3. O'Malley SS: Opioid antagonists in the treatment of alcohol dependence: Clinical efficacy and presentation of relapse. Alcohol Alcohol 1996, 1:77–81.
4. Anton RF, O'Malley SS, Ciraulo DC, Cisler RA, Couper D, Donovan DM, Gastfriend DR, Hosking JD, Johnson BA, LoCastro JS, Longabaugh R, Mason BJ, Mattson ME, Miller WR, Pettinati HM, Randall CL, Swift R, Weiss RD, Williams LD, Zweben AZ, for the COMBINE Study Research Group: Combined pharmacotherapies and behavioral interventions for alcohol dependence: The COMBINE Study: A Randomized Controlled Trial. JAMA 2006, 295:2003–2017
5. Renault PF. Treatment of heroin-dependent persons with antagonists: current status. Bull Narc. 1978 Apr-Jun;30(2):21-9.
6. Krupitsky E, Zvartau E, Masalov D, Tsoy M, Burakov A, Egorova V, Didenko T, Romanova T, Ivanova E, Bespalov A, Verbitskaya EV, Neznanov NG, Grinenko AY, O'Brien CP, Woody GE: Naltrexone with or without fluoxetine for preventing relapse to heroin addiction in St. Petersburg, Russia. J Subst Abuse Treat 2006, 31:319–328.
7. Crabtree BL. Review of naltrexone, a long-acting opiate antagonist. Clin Pharm. 1984 May-Jun;3(3):273-80. PMID: 6329589.
8. O'Malley S, Jaffe AJ, Chang G, Schottenfeld RS, Meyer RE, Rounsaville B: Naltrexone and coping skills therapy for alcohol dependence. Arch Gen Psychiatry 1992, 49:881–887.
9. Volpicelli JR, Rhines KC, Rhines JS, Volpicelli LA, Alterman AI, O'Brien CP: Naltrexone and alcohol dependence: role of subject compliance. Arch Gen Psychiatry 1997, 54:737–742
10. Verebey K, Mulé SJ. Naltrexone pharmacology, pharmacokinetics, and metabolism: current status. Am J Drug Alcohol Abuse. 1975;2(34):357–363.
11. Schmidt WK, Tam SW, Shotzberger GS, Smith DH, Jr, Clark R, Bernier VG. Nalbuphine. Drug Alcohol Depend. 1985;14(34):339–362.
12. Okada T, Le Trong I, Fox BA, Behnke CA, Stenkamp RE, Palczewski K. X-Ray diffraction analysis of three-dimensional crystals of bovine rhodopsin obtained from mixed micelles. J Struct Biol. 2000 May;130(1):73-80.
13. Palczewski K, Kumasaka T, Hori T, Behnke CA, Motoshima H, Fox BA, Le Trong I, Teller DC, Okada T, Stenkamp RE, Yamamoto M, Miyano M. Crystal structure of rhodopsin: A G protein-coupled receptor. Science. 2000 Aug 4;289(5480):739-45.
14. Teller DC, Okada T, Behnke CA, Palczewski K, Stenkamp RE. Advances in determination of a high-resolution three-dimensional structure of rhodopsin, a model of G-protein-coupled receptors (GPCRs). Biochemistry. 2001 Jul 3;40(26):7761-72.
15. Okada T, Fujiyoshi Y, Silow M, Navarro J, Landau EM, Shichida Y. Functional role of internal water molecules in rhodopsin revealed by X-ray crystallography. Proc Natl Acad Sci U S A. 2002 Apr 30;99(9):5982-7.
16. Elling CE, Thirstrup K, Nielsen SM, Hjorth SA, Schwartz TW. Metal-ion sites as structural and functional probes of helix-helix interactions in 7TM receptors. Ann N Y Acad Sci. 1997 Apr 24;814:142-51.
17. Mizobe T, Maze M, Lam V, Suryanarayana S, Kobilka BK. Arrangement of transmembrane domains in adrenergic receptors. Similarity to bacteriorhodopsin. J Biol Chem. 1996 Feb 2;271(5):2387-9.
18. Manglik, A.; Kruse, A. C.; Kobilka, T. S.; Thian, F. S.; Mathiesen, J. M.; Sunahara, R. K.; Pardo, L.; Weis, W. I.; Kobilka, B. K.; Granier, S. Crystal structure of the μ-opioid receptor bound to a morphinan antagonist. Nature 2012, 485, 321−326.
19. Carroll, F. I.; Dolle, R. E. The discovery and development of the N-substituted trans-3,4-dimethyl-4-(3′-hydroxyphenyl)piperidine class of pure opioid receptor antagonists. ChemMedChem 2014, 9, 1638−1654.

20. Yuan, Y.; Zaidi, S. A.; Elbegdorj, O.; Aschenbach, L. C.; Li, G.; Stevens, D. L.; Scoggins, K. L.; Dewey, W. L.; Selley, D. E.; Zhang, Y. Design, synthesis, and biological evaluation of 14-heteroaromaticsubstituted naltrexone derivatives: pharmacological profile switch from mu opioid receptor selectivity to mu/kappa opioid receptor dual selectivity. J. Med. Chem. 2013, 56, 9156−9169.
21. Shang, Y.; LeRouzic, V.; Schneider, S.; Bisignano, P.; Pasternak, G. W.; Filizola, M. Mechanistic insights into the allosteric modulation of opioid receptors by sodium ions. Biochemistry 2014, 53, 5140− 5149.
22. Livingston, K. E.; Traynor, J. R. Disruption of the Na+ ion binding site as a mechanism for positive allosteric modulation of the mu-opioid receptor. Proc. Nat. Acad. Sci. U. S. A. 2014, 111, 18369− 18374.
23. Huang, W.; Manglik, A.; Venkatakrishnan, A. J.; Laeremans, T.; Feinberg, E. N.; Sanborn, A. L.; Kato, H. E.; Livingston, K. E.; Thorsen, T. S.; Kling, R. C.; Granier, S.; Gmeiner, P.; Husbands, S. M.; Traynor, J. R.; Weis, W. I.; Steyaert, J.; Dror, R. O.; Kobilka, B. K. Structural insights into μ-opioid receptor activation. Nature 2015, 524, 315−321.
24. Rasmussen, S. G.; Choi, H. J.; Fung, J. J.; Pardon, E.; Casarosa, P.; Chae, P. S.; Devree, B. T.; Rosenbaum, D. M.; Thian, F. S.; Kobilka, T. S.; Schnapp, A.; Konetzki, I.; Sunahara, R. K.; Gellman, S. H.; Pautsch, A.; Steyaert, J.; Weis, W. I.; Kobilka, B. K. Structure of a nanobody-stabilized active state of the β(2) adrenoceptor. Nature 2011, 469, 175−180.
25. Ring, A. M.; Manglik, A.; Kruse, A. C.; Enos, M. D.; Weis, W. I.; Garcia, K. C.; Kobilka, B. K. Adrenaline-activated structure of β2- adrenoceptor stabilized by an engineered nanobody. Nature 2013, 502, 575−579.
26. Kruse, A. C.; Ring, A. M.; Manglik, A.; Hu, J.; Hu, K.; Eitel, K.; Hübner, H.; Pardon, E.; Valant, C.; Sexton, P. M.; Christopoulos, A.; Felder, C. C.; Gmeiner, P.; Steyaert, J.; Weis, W. I.; Garcia, K. C.; Wess, J.; Kobilka, B. K. Activation and allosteric modulation of a muscarinic acetylcholine receptor. Nature 2013, 504, 101−106.
27. Kapoor, A.; Martinez-Rosell, G.; Provasi, D.; de Fabritiis, G.; Filizola, M. Dynamic and kinetic elements of μ-opioid receptor functional selectivity. Sci. Rep. 2017, 7, 11255.
28. Manglik, A.; Lin, H.; Aryal, D. K.; McCorvy, J. D.; Dengler, D.; Corder, G.; Levit, A.; Kling, R. C.; Bernat, V.; Hübner, H.; Huang, X. P.; Sassano, M. F.; Giguere, P. M.; Löber, S.; Da, D.; Scherrer, G.; Kobilka, B. K.; Gmeiner, P.; Roth, B. L.; Shoichet, B. K. Structurebased discovery of opioid analgesics with reduced side effects. Nature 2016, 537, 185−190.
29. de Waal, P. W.; Shi, J.; You, E.; Wang, X.; Melcher, K.; Jiang, Y.; Xu, H. E.; Dickson, B. M. Molecular mechanisms of fentanyl mediated β-arrestin biased signaling. PLoS Comput. Biol. 2020, 16, No. e1007394.
30. Lipinski, P. F. J.; Jaroń czyk, M.; Dobrowolski, J. C.; Sadlej, J. Molecular dynamics of fentanyl bound to μ-opioid receptor. J. Mol. Model. 2019, 25, 144.
31. Koehl, A.; Hu, H.; Maeda, S.; Zhang, Y.; Qu, Q.; Paggi, J. M.; Latorraca, N. R.; Hilger, D.; Dawson, R.; Matile, H.; Schertler, G. F. X.; Granier, S.; Weis, W. I.; Dror, R. O.; Manglik, A.; Skiniotis, G.; Kobilka, B. K. Structure of the μ-opioid receptor-Gi protein complex. Nature 2018, 558, 547−552
32. Chatterjie N, Inturrisi CE. Stereospecific synthesis of the 6beta-hydroxy metabolites of naltrexone and naloxone. J Med Chem. 1975 May;18(5):490-2.
33. Fazlul Huq , 2006. Molecular Modelling Analysis of the Metabolism of Naltrexone. *Journal of Pharmacology and Toxicology, 1: 354-361.*
34. M.G. Wolf, M. Hoefling, C. Aponte-Santamaría, H. Grubmuller, G. Groenhof, g_membed: Efficient insertion of a membrane protein into an equilibrated lipid bilayer with minimal perturbation, J. Comput. Chem. 31 (2010) 2169– 2174.
35. Ricarte A, Dalton JAR, Giraldo J. Structural Assessment of Agonist Efficacy in the μ-Opioid Receptor: Morphine and Fentanyl Elicit Different Activation Patterns. J Chem Inf Model. 2021 Mar 22;61(3):1251-1274. doi: 10.1021/acs.jcim.0c00890. Epub 2021 Jan 15. PMID: 33448226.
36. Siyan Liao, Kai Tan, Cecilia Floyd, Daegun Bong, Michael James Pino, Chun Wu. Probing biased activation of mu-opioid receptor by the biased agonist PZM21 using all atom molecular dynamics simulation, Life Sciences, 269, 2021, 119026
37. Diniz M. Sena, Xiaojing Cong, Alejandro Giorgetti. Ligand based conformational space studies of the μ-opioid receptor. Biochimica et Biophysica Acta (BBA) - General Subjects, 1865 (3), 2021, 129838
38. Li, J. G.; Chen, C.; Yin, J.; Rice, K.; Zhang, Y.; Matecka, D.; de Riel, J. K.; DesJarlais, R. L.; Liu-Chen, L. Y. Asp147 in the third transmembrane helix of the rat μ opioid receptor forms ion-pairing with morphine and naltrexone. Life Sci. 1999, 65, 175−185.
39. Dalton, J. A.; Lans, I.; Giraldo, J. Quantifying conformational changes in GPCRs: glimpse of a common functional mechanism. BMC Bioinf. 2015, 16, 124.

40. Xu, W.; Sanz, A.; Pardo, L.; Liu-Chen, L. Y. Activation of the mu opioid receptor involves conformational rearrangements of multiple transmembrane domains. Biochemistry 2008, 47, 10576− 10586.
41. Befort, K.; Tabbara, L.; Bausch, S.; Chavkin, C.; Evans, C.; Kieffer, B. The conserved aspartate residue in the third putative transmembrane domain of the delta-opioid receptor is not the anionic counterpart for cationic opiate binding but is a constituent of the receptor binding site. Mol. Pharmacol. 1996, 49, 216−223.
42. Mansour A, Taylor LP, Fine JL, Thompson RC, Hoversten MT, Mosberg HI, Watson SJ, Akil H. Key residues defining the mu-opioid receptor binding pocket: a site-directed mutagenesis study. J Neurochem. 1997 Jan;68(1):344-53.
43. B. Webb, A. Sali. Comparative Protein Structure Modeling Using Modeller. Current Protocols in Bioinformatics 54, John Wiley & Sons, Inc., 5.6.1-5.6.37, 2016.
44. Chen VB, Arendall WB 3rd, Headd JJ, Keedy DA, Immormino RM, Kapral GJ, Murray LW, Richardson JS, Richardson DC. MolProbity: all-atom structure validation for macromolecular crystallography. Acta Crystallogr D Biol Crystallogr. 2010 Jan;66(Pt 1):12-21.
45. M.J. Frisch, G.W. Trucks, H.B. Schlegel, G.E. Scuseria, M.A. Robb, J.R.Cheeseman, G. Scalmani, V. Barone, B. Mennucci, G.A. Petersson, H. Nakatsuji,M. Caricato, X. Li, H.P. Hratchian, A.F. Izmaylov, J. Bloino, G. Zheng, J.L.Sonnenberg, M. Hada, M. Ehara, K. Toyota, R. Fukuda, J. Hasegawa, M. Ishida,T. Nakajima, Y. Honda, O. Kitao, H. Nakai, T. Vreven, J.A. Montgomery Jr., J.E.Peralta, F. Ogliaro, M. Bearpark, J.J. Heyd, E. Brothers, K.N. Kudin, V.N.Staroverov, R. Kobayashi, J. Normand, K. Raghavachari, A. Rendell, J.C. Burant,S.S. Iyengar, J. Tomasi, M. Cossi, N. Rega, J.M. Millam, M. Klene, J.E. Knox, J.B.Cross, V. Bakken, C. Adamo, J. Jaramillo, R. Gomperts, R.E. Stratmann, O.Yazyev, A.J. Austin, R. Cammi, C. Pomelli, J.W. Ochterski, R.L. Martin, K.Morokuma, V.G. Zakrzewski, G.A. Voth, P. Salvador, J.J. Dannenberg, S.Dapprich, A.D. Daniels, Farkas Ö, J.B. Foresman, J.V. Ortiz, J. Cioslowski, D.J.Fox, Gaussian 09, Revision D.01, Gaussian, Inc., Wallingford CT, 2009.
46. Morris, G. M., Huey, R., Lindstrom, W., Sanner, M. F., Belew, R. K., Goodsell, D. S., & Olson, A. J. (2009). AutoDock4 and AutoDockTools4: Automated docking with selective receptor flexibility. Journal of Computational Chemistry, 30(16), 2785–2791.
47. M.A. Lomize, A.L. Lomize, I.D. Pogozheva, H.I. Mosberg, OPM: orientations of proteins in membranes database, Bioinformatics 22 (5) (2006) 623–625
48. S. Jo, T. Kim, W. Im, Automated builder and database of protein/membrane complexes for molecular dynamics simulations, PLoS One 2 (9) (2007) e880.
49. S. Jo, J.B. Lim, J.B. Klauda, W. Im, CHARMM-GUI membrane builder for mixed bilayers and its application to yeast membranes, Biophys. J. 97 (1) (2009) 50– 58.
50. D.A. Case, T.E. Cheatham 3rd, T. Darden, H. Gohlke, R. Luo, K.M. Merz Jr., A. Onufriev, C. Simmerling, B. Wang, R.J. Woods, The Amber biomolecular simulation programs, J. Comput. Chem. 26 (16) (2005) 1668–1688
51. J.A. Maier, C. Martinez, K. Kasavajhala, L. Wickstrom, K.E. Hauser, C. Simmerling, ff14SB: improving the accuracy of protein side chain and backbone parameters from ff99SB, J. Chem. Theory Comput. 11 (8) (2015) 3696–3713.
52. C.J. Dickson, B.D. Madej, A.A. Skjevik, R.M. Betz, K. Teigen, I.R. Gould, R.C. Walker, Lipid14: the amber lipid force field, J. Chem. Theory Comput. 10 (2) (2014) 865–879.
53. J. Wang, R.M. Wolf, J.W. Caldwell, P.A. Kollman, D.A. Case, Development and testing of a general amber force field, J. Comput. Chem. 25 (9) (2004) 1157–1174.
54. Tom Darden, D.Y. Lee Pedersen, Particle mesh Ewald: an N·log(N) method for Ewald sums in large systems, J. Chem. Phys. 98 (12) (1993).
55. W.F. van Gunsteren, H.J.C. Berendsen, Algorithms for macromoleculardynamics and constraint dynamics, Mol. Phys. 34 (5) (1977) 1311–1327
56. W.L. DeLano, The PyMOL Molecular Graphics System, DeLano Scientific, Palo Alto, CA, 2002.
57. Miller, B. R., 3rd; McGee, T. D., Jr.; Swails, J. M.; Homeyer, N.; Gohlke, H.; Roitberg, A. E., MMPBSA.py: An Efficient Program for End-State Free Energy Calculations. *Journal of chemical theory and computation* **2012,** *8* (9), 3314-21.
58. Feig, M., Onufriev, A., Lee, M.S., Im, W., Case, D.A., Brooks, C.L., 2004. Performance Comparison of Generalized Born and Poisson Methods in the Calculation of Electrostatic Solvation Energies for Protein Structures. J. Comput. Chem. 25, 265–284.
59. Bello, M., 2018. Binding mechanism of kinase inhibitors to EGFR and T790M, L858R and L858R/T790M mutants through structural and energetic analysis. Int. J. Biol. Macromol. 118, 1948–1962.